CHARACTERIZING FIELD EMISSION IN ELECTROSTATIC TRACTOR OPERATIONS FOR GEOSYNCHRONOUS ORBIT DEBRIS REMOVAL

A. Haft, E. Weber, and H. Schaub

University of Colorado Boulder, 3775 Discovery Dr., Boulder, CO, USA,
Email: {amy.haft, ethan.weber, hanspeter.schaub}@colorado.edu

ABSTRACT

The accumulation of non-compliant and abandoned satellites in Geosynchronous Earth Orbit (GEO) presents a growing risk of collision events that could threaten critical space-based systems. The electrostatic tractor (ET) has been proposed as a contactless method for active debris removal (ADR) in GEO. This method utilizes an electron beam to induce differential charging between a servicer spacecraft and a debris object, resulting in an attractive electrostatic force that can be used to move the debris to a graveyard orbit. Prior studies have demonstrated that this force can be significantly increased by pulsing the electron beam with an optimal duty cycle, greatly reducing debris deorbit times. However, the high electric potential differences produced by this method can introduce field electron emission (FE), a phenomena where electrons are emitted from sharp surface features due to strong local electric fields. This study explores the effects of field electron emissions during ET operations by characterizing the impacts of surface geometry, duty cycle, and spacecraft proximity on surface electric field and field emission current density though computational finite element analysis and applying these results to a pulsed electron beam charging simulation. Results indicate that the size of surface features has a greater impact on field emissions than the proximity between the servicer spacecraft and debris object, and sufficiently small features could produce field emissions large enough to reduce the performance of the pulsed ET method.

Keywords: Field Electron Emission, Electrostatic Tractor, Active Debris Removal.

1. INTRODUCTION

Geosynchronous Earth Orbit (GEO) is a critical region for global communications, broadcasting, and Earth observation, yet the increasing presence of non-compliant and abandoned satellites poses a growing collision risk [1, 2]. To minimize long-term debris accumulation, the Inter-Agency Space Debris Coordination Committee (IADC) has established guidelines recommending that defunct satellites be relocated to a graveyard orbit several hundred kilometers above GEO. This includes an additional 235 km to account for the GEO-protected zone and external perturbations such as gravitational forces and solar radiation pressure [3]. Despite these recommendations, analysis of satellite disposal between 1997 and 2013 indicates that only about half of all GEO satellites adhered to the guidelines, while nearly 30% fell short of compliance and another 20% were completely abandoned [4]. Regulatory efforts to enforce proper end-of-life disposal have been slow to take effect: the United States Federal Communications Commission (FCC) implemented a policy in 2002 requiring that all GEO satellites launched after March 18 of that year undergo a minimum altitude boost of 300 km before decommissioning [5], but meaningful enforcement mechanisms for this policy were not introduced until 2023 [6]. Given the high financial value of GEO satellites [4], maintaining the long-term sustainability of this orbital regime is crucial. Without stricter adherence to disposal protocols, the continued accumulation of defunct satellites increases the probability of collision events that could threaten critical space-based infrastructure. Addressing the growing debris population in GEO requires dedicated Active Debris Removal (ADR) efforts. Most ADR concepts designed for Low Earth Orbit (LEO) rely on physical contact with the target object, using techniques such as robotic arms, nets,

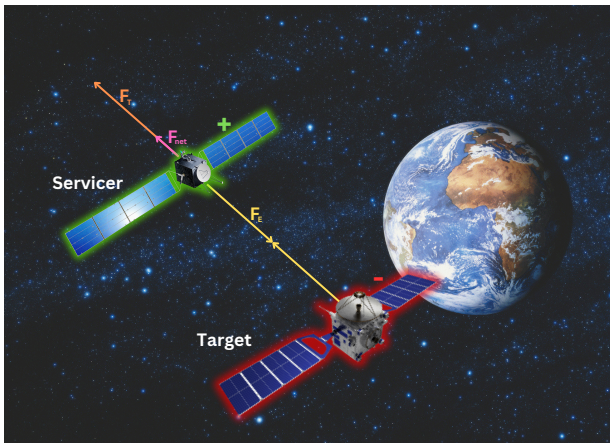

Figure 1: Electrostatic Tractor Concept Figure [7]

or mechanical grappling [8, 9, 10, 11, 12, 13], but these approaches face significant challenges in the GEO environment where abandoned satellites have been observed to be tumbling at rates of tens of degrees per second [14, 15]. High spin rates make direct capture and detumbling extremely complex, reducing the feasibility of physical contact based ADR techniques [16]. To overcome these challenges, alternative non-contact approaches have been explored. One such method, the electrostatic tractor (ET), introduced in 2012 as a potential solution for ADR in GEO [17], involves equipping a servicer spacecraft with an electron gun that directs a beam of electrons toward a target debris object. As electrons are emitted from the servicer and impact the target, a differential charge develops: the servicer becomes positively charged, while the target acquires a negative charge. This results in an electric potential difference and thus an attractive electrostatic force between the spacecraft that allows the servicer to gradually maneuver the debris into a designated graveyard orbit. Unlike in LEO, where electrostatic interactions are significantly limited due to the short Debye length of a few centimeters, the GEO environment offers a Debye length of several hundred meters, ensuring that ambient plasma does not interfere with charge accumulation or electrostatic force generation [18].

Previous studies using a continuous electron beam find that the electrostatic tractor produced an electrostatic force on the order of milli-Newtons or less [19, 20]. In one such study, the electron beam parameters were varied for a range of plasma conditions to find the optimal combination of beam energy and current to maximize the ET force [21]. Reference [22] proposes the use of a pulsed electron beam in order to increase the electrostatic force. The paper theorizes that, for a given electron beam power level, it is possible to achieve higher inter-spacecraft electric potentials by turning the electron beam on for only a fraction of the time while increasing the electron beam current and voltage relative to the duty cycle. Because the inter-spacecraft electrostatic force increases as a function of spacecraft potential, the pulsed beam can theoretically produce a higher electrostatic force than a continuous beam. Reference [22] optimizes the force by varying a tuning parameter that determines the ratio of e-beam current to e-beam voltage. More recently, Reference [7] applies this pulsed electron beam concept and optimized the beam duty cycle to maximize the inter-spacecraft electric potential. The results of this study show that the use of a pulsed electron beam with an optimized duty cycle significantly increased inter-spacecraft electrostatic forces when compared to a continuous beam and reduced the de-orbit times to just a few days when in eclipse in active space environments (down from hundreds of days for a continuous beam). These force increases were the result of extremely high spacecraft potentials, sometimes reaching more than -150kV. While the optimized pulsed-beam shows great promise as a method to increase the efficiency of the ET, the large resulting electric potential differences may introduce considerable risks during its operation.

While arcing between components on the target is not generally a concern when considering space debris removal, self-emission of electrons due to the influence of a strong electric field may impact the safety and effectiveness of the ET method. This phenomenon is known as field emission, and in this case refers specifically to electron emission from the target. The possible consequences of field emission include a reduced target potential, additional negative currents on the servicer, and hazardous arcing between the target and servicer. The goal of this study is to model the field emission from a target spacecraft while using a pulsed electron beam and asses the resulting risks to the operation of the ET. This paper first explores how the radius of curvature of sharp features, such as needles, corners, or asperities, on an isolated target spacecraft impacts the surface electric field. This analysis is performed for various duty cycles using the aforementioned pulsed electron beam study results. Next, the enhancement of the surface electric field at these sharp features due to close proximity to the servicer spacecraft are explored. For simplicity, the servicer is modeled as a sphere and the sharp target features are reduced to a spherical tip. These electric field results are discussed in terms of their implications on field emission. Finally, the paper explores the coupled effects of field emission on time-varying charging.

2. FIELD EMISSION BACKGROUND

Field electron emission, or simply field emission (FE), is the phenomenon through which electrons escape the bonds of a material when they are excited by a strong electric field. FE is often studied in the context of vacuum electronics [23, 24] and nanostructures [25, 26], such as in the development of electron emitters for electric thrusters and nanomaterials like carbon nanotubes. FE technology is also being explored as a method of regulating the charge of spacecraft passing through hot plasma [27]. FE can be modeled using the Fowler-Nordheim (FN) equation [28, 29],

$$J = \frac{A\beta^2 E_a^2}{\Phi} \exp\left(-\frac{B\Phi^{3/2}}{\beta E_a}\right) \tag{1}$$

proposed in 1928 based on metallographic modeling. In this equation, J is the emission current density, E_a is the applied electric field, $A = 1.54 \times 10^{-6}$ A eV V^{-1}, $B = 6.83 \times 10^9$ eV$^{-3/2}$V m^{-1}, Φ is the work function of the material, and β is the field enhancement factor. In this study, the material used is aluminum, which has $\Phi = 4.8$eV [30]. The FN equation above is derived assuming a flat surface, but can be applied to curved surfaces using β, such that

$$E = \beta E_a \tag{2}$$

where E is the local electric field. Using finite element computation, E is calculated directly, so the field enhancement factor β is then applied indirectly as the geometry and other field enhancements will already be taken

into account. Thus, the FN equation becomes

$$J = \frac{AE^2}{\Phi} \exp\left(-\frac{B\Phi^{3/2}}{E}\right). \quad (3)$$

In previous studies exploring the use of FE technology in electric propulsion systems or spacecraft charge control, the space charge limit (SCL) has posed a significant challenge [27]. As electrons are emitted from the cathode surface, they immediately experience their own image charge, creating a field that opposes the applied electric field. As a result, the electrons begin to repel one another, slow down, and sometimes even bounce back to the cathode surface. This hinders the efficiency of the electron emission. One possible solution to mitigate the impact of the SCL is to pulse the emission rather than sending the electrons out in a constant stream, giving the emitted electrons time to redistribute instead of accumulating at the tip. Because the electron beam in this study is always pulsed, the SCL would not notably impact FE and will not be taken into account.

3. PULSED BEAM MODEL

Recent studies have investigated the use of a pulsed electron beam to enhance the electrostatic force between spacecraft [7, 22]. The results of optimizing the duty cycle of the pulsed beam have shown to theoretically reduce the reorbit time of a large defunct GEO spacecraft from several months to less than 5 days while eclipsed during active periods [7]. This promising finding is the result of the e-beam parameters being significantly augmented as a function of the duty cycle, which, in turn, causes the magnitude of the potential of both spacecraft to increase.

For a continuous e-beam, the power equation is $P = IV$ where I is the e-beam current and V is the e-beam voltage. Because the power is fixed, when the e-beam is pulsed, the power equation becomes

$$P = DC\frac{\gamma I}{\sqrt{DC}}\frac{V}{\gamma\sqrt{DC}} \quad (4)$$

where DC is the duty cycle and γ is the tuning parameter. Thus, the resulting $I_{\text{pulsed}} = \frac{\gamma I}{\sqrt{DC}}$ and $V_{\text{pulsed}} = \frac{V}{\gamma\sqrt{DC}}$ increase as the duty cycle decreases.

Reference [7] finds that there is an optimal duty cycle such that the electrostatic force is maximized. This is due to the time it takes to fully charge the spacecraft. When the duty cycle is too small, the target spacecraft does not have time to charge fast enough to reach a higher potential than at the next smallest duty cycle. Thus, the highest potentials and the greatest expected risk of field emission occurs at the optimal duty cycle.

4. FIELD EMISSION AROUND AN ISOLATED SPHERE

Before including the effects of the servicer's electric field, it is crucial to model and understand how the target tip's own electric field is enhanced as the radius of curvature decreases. Modeling the target tip as an isolated sphere, the electric field will increase inversely proportionally to the sphere's radius. This can be expected because

$$E = -\nabla V = -\frac{\mathrm{d}V}{\mathrm{d}R} \quad (5)$$

where $V = kQ/R$ and k is the Coulomb constant, Q is the total charge, and R is the radius of the sphere. From here, the derivative of V with respect to R is

$$E = \frac{kQ}{R^2} = \frac{V}{R}, \quad (6)$$

which tells us that E is inversely proportional to R.

This analytical result is corroborated by computational FEA analysis using COMSOL, a multi-physics simulation tool. The results of this computation analysis are seen in Figure 2a. This figure shows the `log10` of the electric field generated by an isolated sphere in a vacuum with radii ranging from 0.5 mm to as small as 1μm. As expected, the E-field grows super-exponentially as the radius decreases. The E-field is also shown as a function of duty cycle. This is related to Reference [7], which finds an optimal duty cycle to produce the strongest electrostatic force, and thus the largest difference in spacecraft potentials. Therefore, each duty cycle pertains to a specific combination of target and servicer potentials. These potentials are taken for e-beam nominal parameters $I = 520\mu$A and $V = 40$ kV for spacecraft in eclipse during an active GEO environment, $Kp = 6$ and local time at 4. The peak E-field at each radius applies to the optimal duty cycle, which is 4.489%. While the potentials have some affect on the E-field, the changing radius is a much more significant contributor to enhancing the E-field, which is expected by Equation 6.

The emitted current density corresponding to the E-fields in Figure 2a is show in Figure 2b. Again the the z-axis is represented in its `log10` form for clarity. Here, J was calculated by plugging the E-field at each point into Equation 3. Because J grows linearly as the radius decreases, the original function is exponential. At the peak duty cycle, the `log10` of J is negative until the radius reaches approximately 0.06 mm. Here, $J \approx 10$ A/m^2. When the radius is less than this, J quickly becomes small, reaching a minimum value of 10^{-81}. At the smallest radius represented in the figure, 1μm, J nearly reach 10^{16} A/m^2, at which point a theoretical nearby spacecraft would most likely experience an arc.

Previous studies find that vacuum breakdown occurs when the current density at the cathode reaches values on the order of 10^{12} A/m^2[31, 23, 32]. At this current density, the cathode begins to melt and is no longer a controllable field emission cathode [23]. At the optimal duty

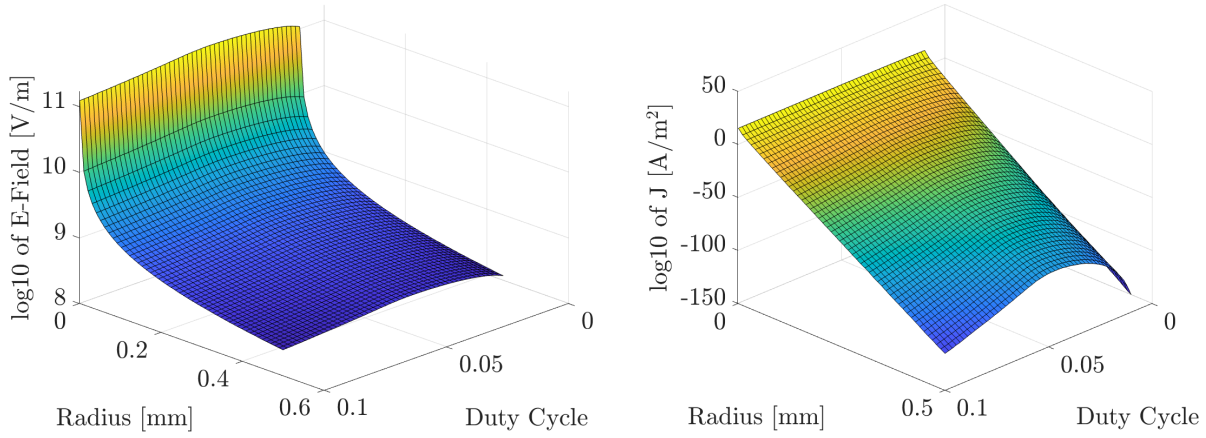

(a) E-field *(b) Current Density*

Figure 2: Isolated Sphere Surface E-field and Current Density vs. Tip Radius and Duty Cycle

cycle, this current density is achieved for a radius of approximately 0.01 mm. This means that for the isolated sphere, explosive electron emission would occur at radii of 0.01 mm and smaller. If an anode was present, arcing would occur for the same range of radii. In a plasma such as GEO, electrical arcing would likely occur before this point because plasma is already ionized and conductive. Thus, 10^{12} A/m^2 is a very conservative estimate for when arcing would begin.

5. FIELD EMISSION IN PROXIMITY OF SERVICER SPACECRAFT

5.1. E-field Enhancement

As the target spacecraft comes within the proximity of the servicer, its local electric field will interact with that of the servicer. Because the target is charged negatively, its electric field points inwards, toward itself. The servicer is charged postively, so its electric field points away from it. In other words, the servicer's electric field serves as an additional applied electric field on the target. The interaction of the electric fields can be roughly modeled by

$$E = E_T + E_S = \frac{V_T}{R_{\text{tip}}} + \frac{V_S}{d - R_T} \tag{7}$$

where V is the electric potential, R is the radius, and the subscripts T and S correspond to the target and servicer, respectively. Thus, proximity to the servicer acts as an electric field enhancement for the target's local electric field.

Figure 3 demonstrates this analytical finding for the 0.1 mm sphere FEA simulation at the peak duty cycle, where the servicer radius is .5 m. A curve, shown in red, of the form $x + y + \exp(-zd)$ – where $x = 9.2228$,

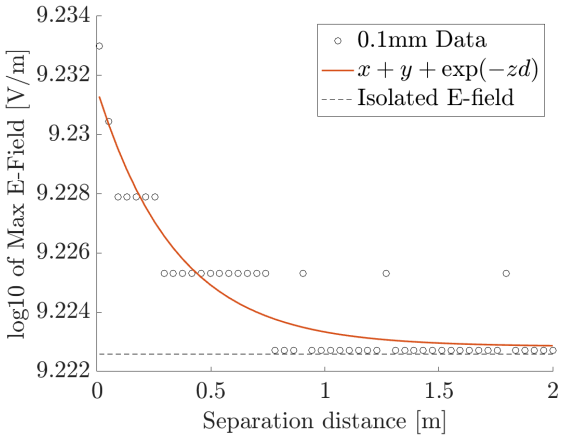

Figure 3: E-field v. Separation Distance for 0.1mm Radius Tip

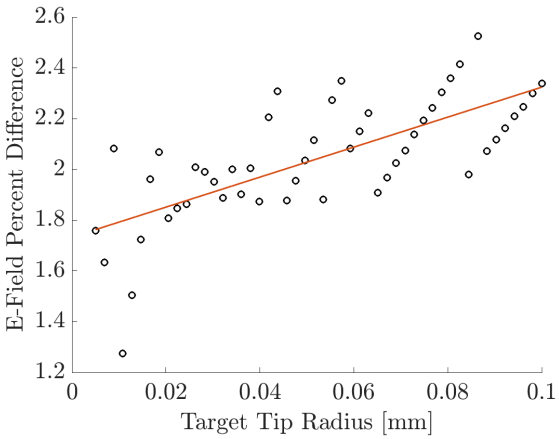

Figure 4: E-field Percent Difference Over Separation Distance v. Tip Radius

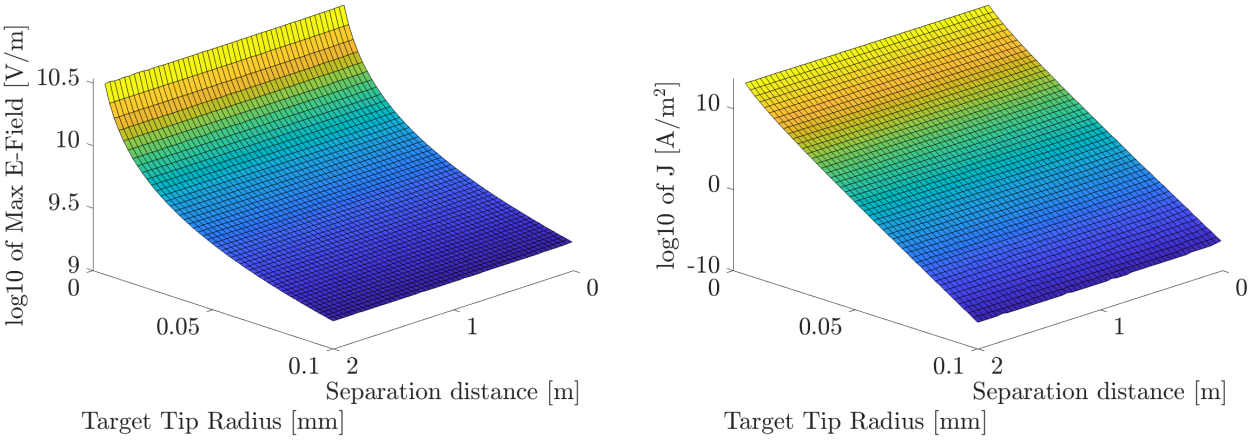

(a) E-field *(b) Current Density*

Figure 5: Surface E-field and Current Density vs. Tip Radius and Spacecraft Separation Distance

$y = 0.0087$, and $z = 2.8713$ and d is the separation distance – is fitted to the data points. The separation distances range from 1cm to 2 m. The curve fitting shows that the E-field decreases as the separation distance increases. The x-asymptote of the curve corresponds to the E-field result for the isolated sphere. The E-field increases from $10^{9.2226}$ V/m isolated to $10^{9.233}$ V/m at 1cm separation distance.

Because the target tip is conductive, the presence of the servicer's E-field causes the surface charges to rearrange themselves such that negative charges accumulate on the side facing the servicer. This causes the charge density on that side to increase compared to the side facing away from the servicer, which, in turn, causes the maximum E-field on the tip to increase. However, as the tip becomes small, this effect is less pronounced as the potential gradient around the tip is also small. Thus, the tip acts more like a point charge as it becomes small. As a result, the maximum E-field increases more dramatically for larger tip radii than for smaller tip radii. This is illustrated in Figure 4, which shows the percent difference between the E-field at 1cm and at 2 m for tip radii ranging from 5μm to 0.1 mm. The linear curve fit shown in red illustrates the increasing E-field percent difference over the range of tip radii. At 5μm, the E-field increases by approximately 1.76% as it is moved inward from 2 m to 1cm. However, at 100μm, the E-field increases by approximately 2.34%.

The results find that tip radius has a significantly larger impact on field enhancement than the distance from the servicer. In Figure 5a, the enhancement due to separation distance is minimal compared to the impact of radius of curvature. Figure 5 shows radii from ranging from 5μm to 0.1 mm and separation distances from 1cm to 2 m. The E-field and J values are represented in their `log10` form as in Figure 2. The resulting E-field values are comparable to that of the isolated sphere, without much noticeable augmentation.

Figure 5b further highlights this finding. At 0.05 mm, the emitted current density is $J = 10^{13.657}$ A/m^2 at $d = 1$cm and $J = 10^{13.625}$ A/m^2 at $d = 2$ m. At the same radius for the isolated sphere, the emitted current density is $J = 13.622$ A/m^2. Using 10^{12} as the threshold for vacuum breakdown, arcing (or explosive electron emission) would occur at this radius regardless of proximity to the servicer. It is found that arcing theoretically occurs for radii of 0.01 m and less regardless of separation distance.

5.2. Effect on Time-Varying Charging

Using the same technique as in Reference [7], the time-varying charging with the pulsed beam is modeled. This time, however, the field emission current is accounted for. The servicer is modeled as a sphere with a 1.5 m radius, and the target is modeled as a sphere with a 4 m radius. An asperity on the target is modeled as a sphere with varying radius sizes. The electric field at the asperity is modeled over time using Equation 7. It was shown that the results from the simulations represented in Figure 5 matched well with the analytical results from Equation 7, so it would produce a good approximation compared to the simulated values.

Figure 6 shows the results from the time-varying simulation. The nominal (unpulsed) e-beam parameters are $I = 520\mu$A and $V = 40$kV. The data is generated for a duty cycle of 5%. The tip radii in the simulation are $5, 10, 30,$ and 50μm. The target and servicer potentials shown in Figures 6a and 6b, respectively, are also computed with the field emission current turned off for reference. This is shown as a black dashed line. In the model, it is assumed that all electrons that are emitted from the target are attracted to the servicer. The emitted current is calculated using $I_{\text{emitted}} = J * A$ where A is the surface area of the tip.

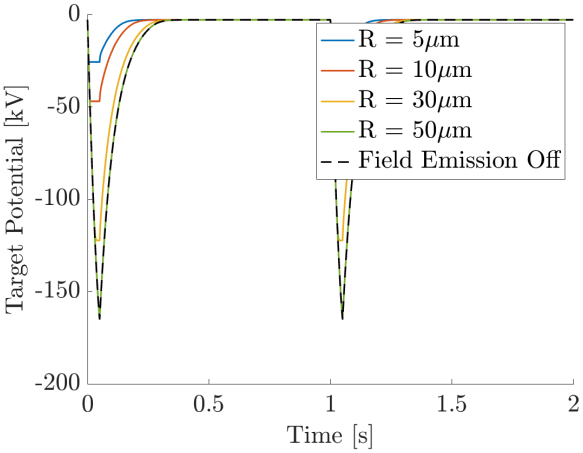

(a) Target Potential vs. Time

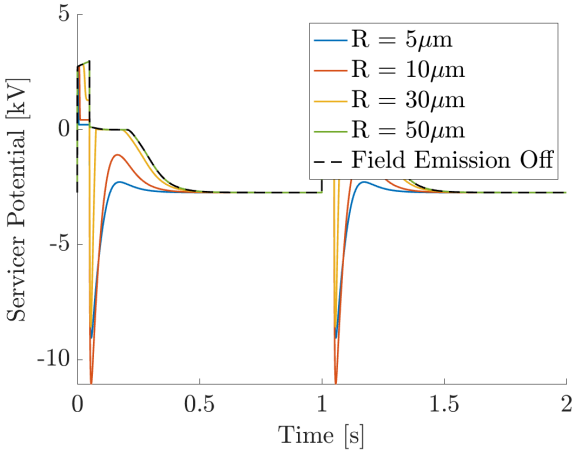

(b) Servicer Potential vs. Time

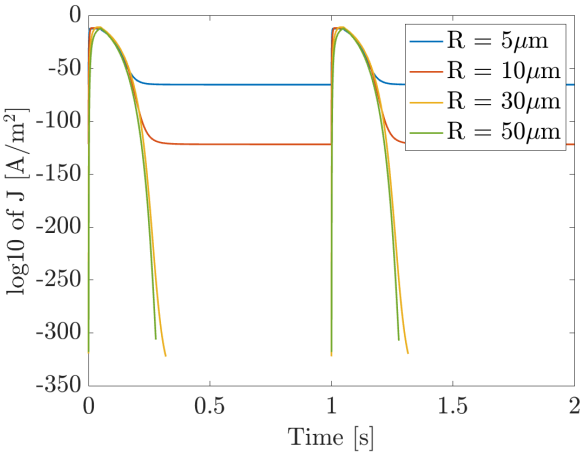

(c) log10 of Current Density vs. Time

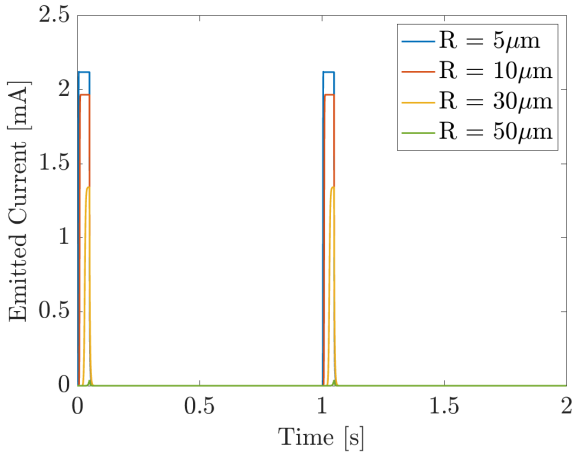

(d) Emitted Current vs. Time

Figure 6: Time-Varying Charging Results with Field Emission

It can be observed in Figure 6a that field emission due to small asperities results in decreased charging. With the tip radius of 5μm, the target charges to only -25.6kV. On the other hand, the target charges to -165kV when the tip radius is 50μm, which is equivalent to the charging of the target without accounting for field emission. This corresponds to the magnitude of emitted current at each radius, shown in Figure 6d. As the radius of the tip increases, the amount of emitted current decreases. At 50μm, the emitted current is near zero. Likewise, the servicer charges negatively when impacted by the emitted current, as seen in Figure 6b. For smaller radii, this effect is more profound since there is more current emitted from the tip.

Notably, these time-varying results show that arcing is not a concern. While field emission reaches relatively high currents for small tip radii, the current density remains low. The current density does not exceed 10^{-11}. This maximum current density interestingly occurs for the 30μm radius, but all of the radii reach similar maxima. Therefore, even though the target charges to extremely large potentials, the 50μm radius tip does not pose a risk of arcing. Moreover, the 50μm radius tip mitigates decreased charging related to field emission and prevents the servicer from reaching negative potentials. This indicates that field emission is only a concern for small enough geometrical features.

6. CONCLUSION

This study investigates the field emission from a spherical spacecraft tip, which represents any sharp geometrical features. When modeling the tip as isolated in a vacuum, it is found that the spacecraft potential has a minor impact on enhancing the electric field compared to the tip radius. With the spacecraft potential fixed at each data point, explosive electron emission is a risk for radii smaller than 0.01mm.

Of interest is the field emission that occurs between two charged spacecraft, particularly when actively amplifying their potentials using a pulsed electron beam. Compared to the isolated case, it was expected that proximity to the servicer spacecraft would cause the electric field to be further enhanced. However, it is found that while this effect exists, it is negligible compared to that from the radius of the tip.

When modeling the pulsed electron beam over time and calculating the time-varying field emission, it is found that the most significant effects are decreased target charging and negative servicer charging. While this does not result in repulsive forces due to induced charging effects, it does cause the force to be nullified during the periods the servicer potential is negative. This means that field emission could hinder the performance of the electrostatic tractor and increase the reorbit time. However, this effect is not felt for larger tip radii, at which point the charging behaves identically to the case not accounting for field emission. Conclusively, small enough spacecraft features and asperities could nullify the positive effects of the pulsed electron beam.

Future work would determine the effects of edges and corners on field emission during active spacecraft charging. It is of interest to find if these features would result in decreased charging. This work would ultimately find whether the pulsed electron beam would prove advantageous for typical spacecraft geometries.

7. ACKNOWLEDGMENTS

The authors would like to thank Dr. Tejaswi Shinde for her guidance using the necessary software for this study. This work was supported by the U.S. Air Force Office of Scientific Research under grant FA9550-23-S-0570.

REFERENCES

1. Zhang H, Li Z, Wang W, Zhang Y, and Wang H. Geostationary orbital debris collision hazard after a collision. Aerospace 5 2022;9:258.
2. Oltrogge DL, Alfano S, Law C, Cacioni A, and Kelso TS. A comprehensive assessment of collision likelihood in Geosynchronous Earth Orbit. Acta Astronautica 2018;147:316–45.
3. IADC Space Debris Mitigation Guidelines. Tech. rep. Inter-Agency Debris Coordination Committee, 2007.
4. Schaub H, Jasper LEZ, Anderson PV, and McKnight DS. Cost and risk assessment for spacecraft operation decisions caused by the space debris environment. Acta Astranautica 2015;113:66–79.
5. de Selding P. FCC Enters Orbital Debris Debate. Space News Business Report 2004.
6. Shepardson D. DISH gets first-ever space debris fine over EchoStar-7. Reuters 2023.
7. Haft A and Schaub H. Increasing the Electrostatic Force Between Spacecraft Using a Pulsed Electron Beam. In: *AAS Space Flight Mechanics Meeting*. 2025.
8. Reintsema D, Thaeter J, Rathke A, et al. DEOS – The German Robotics Approach to Secure and De-Orbit Malfunctioned Satellites from Low Earth Orbits. In: *i-SAIRAS*. August 29-September 1, Sapporo, Japan. 2010.
9. Biesbroek R, Aziz S, Wolahan A, et al. The Clearspace-1 Mission: ESA and Clearspace Teap Up To Remove Debris. In: *8th European Conference on Space Debris*. 2021.
10. Nishida SI and Kawamoto S. Strategy for capturing of a tumbling space debris. Acta Astronautica 2011;68:113–20.
11. Stadnyk K, Hovell K, and Brewster L. Space Debris Removal With Sub-Tethered Net: A Feasibility Study and Preliminary Design. In: *8th European Conference on Space Debris*. 2021.
12. Dudziak R, Tuttle S, and Barraclough S. Harpoon technology development for the active removal of space debris. Advances in Space Research 2015;56:509–27.
13. Aglietti GS, Taylor B, fellowes S, et al. The active space debris removal mission RemoveDebris. Part 2: In orbit operations. Acta Astronautica 2020;168:310–22.
14. Papushev P, Karavaev Y, and Mishina M. Investigations of the evolution of optical characteristics and dynamics of proper rotation of uncontrolled geostationary artificial satellites. Advances in Space Research 9 2009;43:1416–22.
15. Karavaev Y, R.M.Kopyatkevich, Mishina M, Mishin G, Papushev P, and Shaburov P. The dynamic properties of rotation and optical characteristics of space debris at geostationary orbit. Advances in the Astronautical Sciences 2004:1457–66.
16. Trevor Bennett Daan Stevenson EH and Schaub H. Prospects and challenges of touchless electrostatic detumbling of small bodies. Advances in Space Research 2015;56:557–68.
17. Schaub H and D. F. Moorer J. Geosynchronous large debris reorbiter: Challenges and prospects. The Journal of Astronautical Sciences 2012;59:161–76.
18. Champion K and Schaub H. Electrostatic Potential Shielding in Representative Cislunar Regions. IEEE Transactions on Plasma Science 9 2023;51:2482–500.
19. Hammerl J and Schaub H. Reduced Order Spacecraft Charging Models for Electrostatic Proximity Operations. IEEE Transactions on Plasma Science submitted.

20. Haft A and Schaub H. Electrostatic Tractor Effectiveness in a Non-Maxwellian GEO Plasma Environment. In: *AAS Astrodynamics Specialist Conference*. 2024.
21. Hogan EA and Schaub H. Impacts of Hot Space Plasma and Ion Beam Emission on Electrostatic Tractor Performance. IEEE TRANSACTIONS ON PLASMA SCIENCE 9 2015;43.
22. Hughes J and Schuab H. Prospects of Using a Pulsed Electrostatic Tractor With Nominal Geosynchronous Conditions. IEEE Transactions on Plasma Science 2017;45.
23. Fursey GN. Field emission in vacuum microelectronics. Applied Surface Science 1-4 2003;215.
24. Egorov N and Sheshin E. Field Emission Electronics. Springer, 2017. DOI: 10.1007/978-3-319-56561-3. URL: https://link.springer.com/book/10.1007/978-3-319-56561-3.
25. Fang X, Bando Y, Gautam UK, Ye C, and Golberg D. Inorganic Semiconductor Nanostructures and Their Field-Emission Applications. Journal of Materials Chemistry 2008;18:509–22.
26. Pathak M, Mutadak P, Mane P, et al. Enrichment of the Field Emission Properties of $NiCo_2O$ Nanostructures by UV/O Treatment: Experimental and Theoretical Insights. Materials Advances 2021;2:2242–51.
27. Morris D and Gilchrist B. Electron Field Emission and the Space Charge Limit: Techniques and Tradeoffs. In: *39th AIAA/ASME/SAE/ASEE Joint Propulsion Conference and Exhibit*. Huntsville, Alabama: American Institute of Aeronautics and Astronautics (AIAA), 2003. DOI: 10.2514/6.2003-4792.
28. Fowler RH and Nordheim L. Electron Emission in Intense Electric Fields. Proceedings of the Royal Society A: Mathematical, Physical and Engineering Sciences 781 1928;119:173–81.
29. Chen Y, Liu Z, Xiao Z, et al. Processing, property modulation and application of one-dimensional SiC nanostructure field emitters. Microelectronic Engineering 2023;277:112019.
30. Michaelson HB. The Work Function of the Elements and its Periodicity. Journal of Applied Physics 11 1977;48.
31. Lafferty JM. Encyclopedia of Physical Science and Technology (Third Edition). In: Elsevier Science Ltd., 2003. Chap. Vacuum Arcs.
32. Jüttner B. Cathode spots of electric arcs. Journal of Physics D: Applied Physics 2001;34.